International Journal of Technology

http://ijtech.eng.ui.ac.id

Research Article

High-Resolution Neutron Diffraction Analysis of Residual Stresses in Oxide Dispersion Strengthened FeNiCrY_2O_3 Cast Alloys for Advanced Nuclear Reactor Applications

Parikin Farihin [1,2,*], Bambang Suharno [1], Ferhat Aziz [2], Mohammad Dani [2], I Wayan Ngarayana [2], Andryansyah [2], Andon Insani [3], Rai Indra Wardana [4], Damar Rastri Adhika [5], Ching An Huang [6]

[1]Department of Metallurgical and Materials Engineering, Faculty of Engineering, University of Indonesia, Depok 16424, West Java, Indonesia.
[2]Research Organization for Nuclear Energy, Nuclear Power Research Organization, National Research and Innovation Agency, BJ Habibie Integrated Science Area Building No. 80, Serpong, Tangerang Selatan 15312, Indonesia
[3]Research Center for Radiation Detection and Nuclear Analysis, Nuclear Power Research Organization, National Research and Innovation Agency, BJ Habibie Integrated Science Area Building No. 80, Serpong, Tangerang Selatan 15312, Indonesia
[4]Bali Region Research and Innovation Agency (BRIDA Bali), Jl. Melati No.23, Dangin Puri Kangin, Denpasar, Bali 802, Indonesia
[5]Research Center for Nanosciences and Nanotechnology, Bandung Institute of Tech., Jl. Ganesha 10, Bandung, West Java 40132, Indonesia
[6]Departement of Mechanical Engineering, Chang Gung University, Taoyuan 33302 Taiwan
**Corresponding author: pari001@brin.go.id, Tel.: +62 0217560912; Fax. : +62 0217560912*

Abstract: High-temperature resistant materials have been developed, including Fe-base austenitic steel with high Ni-Cr content. These materials are modified into oxide dispersion strengthened (ODS) steel incorporated with a small amount of rare earth element (REE) oxides. ODS alloys are a mixture of a metal matrix with uniformly distributed small oxide particles. The alloys show great promise as structural materials for modern engineering applications in advanced- energy and nuclear reactors. A comprehensive understanding of individual mechanical properties and residual stress distribution remains elusive. Therefore, this research aimed to show the influence of Y_2O_3 dispersion on the crystal structure and residual stress in FeNiCr Y_2O_3 cast alloys with varying ODS compositions ranging from 0 to 2.0 wt.% Y_2O_3. Alloys were synthesized by powder metallurgy and melt casting followed by characterization using neutron diffraction as well as standard metallographic methods. During analysis, neutron was powerful for probing solid materials, among other things. The product penetrated deep inside, which made it possible to research bulk properties and internal structures of thick samples or materials encased in containers. Diffraction profile analysis showed that cast alloys signified 'matrix-cluster' composite crystal morphology and improved elemental mapping of the microstructure. Moreover, stress-strain curves moderately estimated optimum Y_2O_3 content to be 1.0 wt.%. Y_2O_3 dispersion induced lattice compression in the austenitic FeNiCr matrix, signifying tensile residual stress in the crystals. Distribution of residual stress in alloys was related to mechanical and

This work was supported by the 'Badan Riset dan Inovasi Nasional' funded by 'RIIM 2023 Batch-3'

https://doi.org/10.14716/ijtech.v16i2.7241
Received August 2024; Revised December 2024; Accepted January 2025

performance properties. In conclusion, most recommended materials for further fabrication as FeNiCr Y_2O_3 ODS cast alloys was 57Fe25Ni17Cr1.0Y_2O_3 system.

Keywords: FeNiCrY_2O_3 ODS casting; Microstructure; Neutron diffraction; Residual stress; Y_2O_3

1. Introduction

Materials suitable for high-temperature environments are advanced nuclear reactors (Was et al., 2019; Zinkle and Was, 2013), which mainly include ferritic and martensitic (F/M)-type superalloy steels. These materials show poor creep properties and have lower resistance to swelling at high temperatures compared to superalloy austenitic steel contrast. Superalloy austenitic steel has a lower hardness than ferritic and martensitic steel, signifying that its toughness still requires improvement. This behavior improves the addition of nano- or micro-powders of rare earth elements (REE), such as Yttria (Y_2O_3), leading to 'oxide dispersion strengthened' (ODS) steel alloys. The hardness of ODS materials increases due to nano-dispersion of Yttria grains, which helps prevent dislocation movement during creep deformation (Du et al., 2024; Xu et al., 2023; Kishorekumar et al., 2018).

The search for advanced materials that can withstand extreme conditions is challenging and has attracted much interest in designing as well as developing advanced nuclear reactors (Aziz et al., 2024; Gougar et al., 2020; Buckthorpe, 2017; Zinkle and Was, 2013). Defining temperature limits is critical for safety requirements, for normal or abnormal operations. This occurs because corrosion at high temperatures has a direct impact on the other mechanical parameters important for safety (Zhang et al., 2019). Numerous candidate materials are investigated for individual use in a high-temperature environment (Yusupandi et al., 2024; Arshad et al., 2022). Among the potential candidates, austenitic stainless steel (ASS) alloys, particularly 56Fe25Ni16.55Cr composition, which is later refined to 58Fe25Ni17Cr, show further improvement. This increment showed resistance to high-temperature corrosion up to 850°C at a rate of 0.06 mm/year (Mustofa et al., 2020; Dani et al., 2020; Parikin et al., 2019). Research to improve the performance of the model by incorporating a rare earth metal oxide, Y_2O_3, has been investigated (Parikin et al., 2021).

Some high-temperature resistant materials, such as 58Fe25Ni17Cr austenitic steel with high Ni-Cr content, have been recently developed (Dani et al., 2019). FeNiCr-based superalloy steels have further been developed to ODS alloys through melt-casting, instead of through powder metallurgy methods (Raman et al., 2016). Moreover, synthesis by a pre-linking method was introduced (Parikin et al., 2024), in which Fe+Y_2O_3 variable-dependent composition was designed to be physically adjacent to cast alloys. Due to varying melting temperatures of main components of alloys (Fe, Ni, Cr, and Y_2O_3) the components develop separately into two distinct phases, i.e. fcc-austenite (FeNiCr) and cubic (Y_2O_3), forming composite materials with unique morphology. However, the presence of these oxide particles in the matrix introduces residual stress impacting reliability and performance of materials (Brewer et al., 2015; Ruan et al., 2012; Oka et al., 2007).

Neutron diffraction method is a powerful non-destructive method for characterizing residual stress in crystalline materials. An overview of the application of neutron diffraction methods in residual stress analysis has been described in (Parikin et al., 2009). Additionally, neutron has a high penetration depth in many materials, allowing research of bulk properties and internal structures of thick samples or materials encased in containers. Different from neutron, X-rays have much lower penetration depth, making the procedure more suited to surface analysis or thin samples. Following this discussion, residual stress is a major factor influencing microstructure and mechanical properties that can be beneficial or detrimental depending on sign, magnitude, as well as loading conditions (Zang et al., 2024; Andoko et al., 2024; Naserinejad et al., 2023; Guo et al., 2020; Li et al., 2019). Under tensile conditions, residual tensile stress on surfaces poses a risk, potentially causing fatigue-induced crack growth (Dong et al., 2023; Kühne et al., 2021; Statti et al., 2021). To address this issue, diffraction methods, particularly neutron diffraction, can be used to examine lattice of strains (Em et al., 2024; Yan et al., 2022; Mo et al., 2018; Tanaka et al., 2002).

This research aims to obtain ODS cast alloy, specifically $FeNiCrY_2O_3$ as superior materials for high-temperature applications. The objective of the analysis is to measure lattice crystals and analyze residual stress in ODS alloys using neutron diffraction and Rietveld analyses. By systematically investigating different oxide contents in $FeNiCrY_2O_3$ ODS cast alloys, correlations between residual stress and microstructure properties with mechanical properties can be developed.

2. Methods

2.1. Used materials for experiments

The initial precursors used to synthesize $FeNiCrY_2O_3$ ODS cast alloys were shown in Table 1. Pure Fe and Cr powders were supplied by Alfa Aesar with purities of 98 and >99, 99.8, and 99.99%. Following the analysis of this research, each precursor had a varying property. The manufacture of samples of ODS cast alloys began with weighing the high-purity powder, using a precision balance. During the process, a one-hour pre-linking method and a twenty-hour planetary ball mill were applied to mix a minimal amount of Y_2O_3 oxide for uniform dispersion in cast alloys with a homogeneous particle size Figure 1. Subsequently, the synthesis was conducted according to the scheme presented in the Figure and described chronologically hereafter.

Table 1 Composition of the initial high-purity precursors used to synthesize ODS $FeNiCrY_2O_3$ alloy

Powder	Purity	Crystal Structure (at 25°C)	Particle Size (μm)	Density ($g.cm^{-3}$)	Melting point (°C)	Source
Fe	98%	*bcc*	44.00	7.80	1535	Alfa Aesar, US
Cr	>99%	*bcc*	44.00	7.14	1435	Alfa Aesar, US
Ni	99.8%	*fcc*	45.00	8.90	1907	Sigma-Aldrich, US
Y_2O_3	99.99%	*cubic*	0.05	5.01	2410	Sigma-Aldrich, US

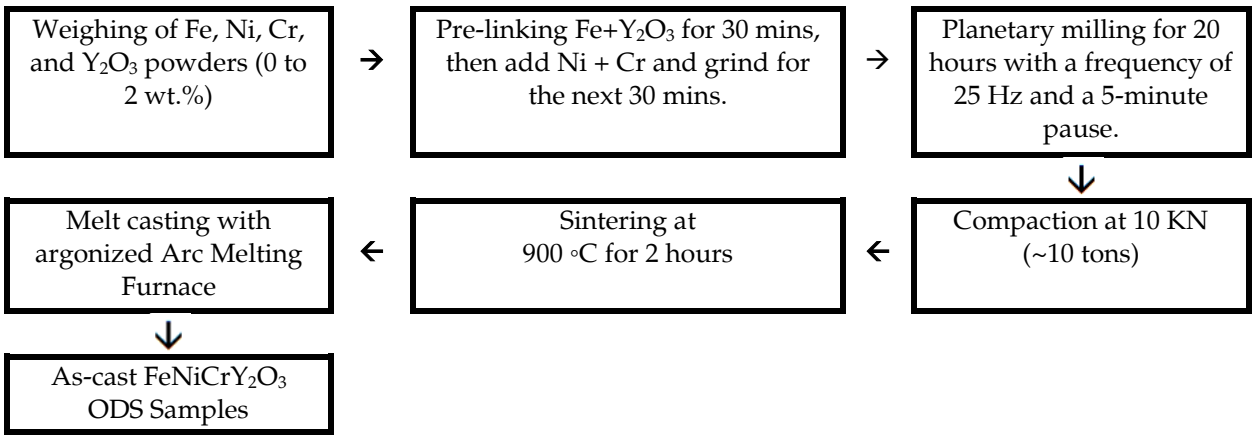

Figure 1 Schematic showing preparation of $FeNiCrY_2O_3$ cast alloys with ODS compositions varying from 0 to 2.0% by weight of Y_2O_3

2.2. Mechanical alloying

The composition of added Y_2O_3 powder was adjusted to match the reduction in composition of Fe powder. High-grade metal powders of Fe, Cr, Ni, and Y_2O_3, as shown in Table 2, were used in casting process. In addition, 25-gram precursor was prepared using $Fe+Y_2O_3$ pre-linking route, which included crushing and grinding in a mortar for 30 minutes manually.

Table 2 Chemical composition of synthesized ODS $FeNiCrY_2O_3$ specimens. The specimens were obtained by vacuum electric arc furnace (EAF) of mechanically alloyed powders

Specimen	Composition (wt.%)			
	Fe	Ni	Cr	Y_2O_3
FeNiCr	58.0	25.0	17.0	0.0
FeNiCr-03Y_2O_3	57.7	25.0	17.0	0.3
FeNiCr-05Y_2O_3	57.5	25.0	17.0	0.5
FeNiCr-07Y_2O_3	57.3	25.0	17.0	0.7
FeNiCr-10Y_2O_3	57.0	25.0	17.0	1.0
FeNiCr-15Y_2O_3	56.5	25.0	17.0	1.5
FeNiCr-20Y_2O_3	56.0	25.0	17.0	2.0

Since Fe was the dominant element in system of alloys, Y_2O_3 grains were close to Fe grains (Parikin et al., 2024). Subsequently, Ni and Cr powders were continuously added as well as subjected to crushing grinding for an additional 30 minutes. Finally, mechanical grounding for 20 hours in Planetary Mill with ball-to-powder ratio of 12:1 and frequency of 25 Hz—5 mins pause was applied.

2.3. Sintering and Smelting

The milled powder was compacted into pellets, each with diameter of 10 mm and thickness of 5 mm, using hydraulic pressurizer (Instron 5569) with pressure of 100 kN which was equivalent to 10 tons load. These pellets were subsequently sintered in vacuum furnace (Carbolite Gero HTRV 16/75/550) at temperature of 900 °C for 2 hours. This sintering process was performed to consolidate the powder and improve the bonding between metal matrix as well as oxide particles. Following sintering, pellets were smelted in an EAF operating at current of 200 A and voltage of 18 V, with an argon flow of 3.5 bars. Ingot specimen was flipped four times during smelting process to ensure uniform heating and melting.

2.4. Characterization Methods

2.4.1. Microstructure observation

Microstructure of the specimens was examined using a variety of microscopy methods. These processes included Olympus BX51DP26 Light Optical Microscope (LOM), Jeol SEM 2650LA Scanning Electron Microscope (SEM) equipped with Energy-Dispersive X-ray Spectroscopy (EDX) detector, and Hitachi HT7700 Transmission Electron Microscope (TEM). The specimens during the analysis were prepared following standard metallography procedure. Initially, the specimens experienced surface grounding using abrasive papers of different grit sizes, ranging from coarse (80) to fine grain (5,000). This procedure was followed by polishing process conducted on pad covered with diamond powder paste with particle size of 1.0 µm. When the surfaces were smooth, the specimens were carefully cleaned using alcohol. The specimens were then etched using an aqua-regia solution for 1-2 minutes to identify individual microstructures. In addition to these procedures, Hitachi FIB 2200 Focused Ion Beam (FIB) was used for the preparation of TEM specimens. This comprehensive method ensured a detailed and accurate observation of microstructure of specimens.

2.4.2. High-resolution neutron powder diffraction

Crystal structure of specimens of $FeNiCrY_2O_3$ ODS cast alloys was examined using Sumitomo Rigaku high-resolution neutron powder diffractometer (HRPD) at G.A, and Siwabessy Research Reactor (RSG-GAS) which was operated at power of 15 MW. The solid weight of each deployed melt-cast ODS specimen ranged from 6 to 8 grams. Additionally, NPD (new products development) data were collected using a wavelength of 1.82 Å with 2θ ranging from 2.5° to 162.5°.

2.4.3. Rietveld analysis

Rietveld analysis commonly called Rietveld refinement was a method in crystallography that was generally used to smoothen crystal structure models by matching all powder neutron and X-ray diffraction patterns through the powder. This method was widely used in determining crystal structure of materials and was capable of providing information i.e., atomic positions, thermal vibrations, diffraction planes, crystallite size, and lattice spacings.

NPD data were analyzed using Rietveld method to obtain lattice and anisotropic mean-square displacement (U) parameters for each phase as well as specimen. Average strain (ε_{av}) and average stress (σ_{av}) were calculated from these parameters. During the process, structural data analysis was conducted using a Rietveld structure refinement program, and Materials Analysis Using Diffraction (MAUD). This MAUD program analyzed diffraction spectra and obtained the structure of crystal, quantity, phase microstructure, texture, as well as residual stress of materials (Lutterotti, 2000). The initial lattice and U parameters to conduct Rietveld analysis for each specimen were shown in Table 3.

3. Results and Discussion

3.1. Microstructure Observations

3.1.1. Optical microscopy

Figure 2 showed the effect of Y_2O_3 dispersion on microstructure of melt-casted FeNiCrY_2O_3 ODS alloys. FeNiCr cast alloys without Y_2O_3 dispersion, as shown in (a), signified needle-like grains that were typical for ASS. The grains were also visible in FeNiCr alloys with 0.3 and 0.5 wt.% Y_2O_3 dispersion. However, with the increase of Y_2O_3 content, the needle-like grains were transformed into circular dendritic formations with wider grain boundaries, as shown in the specimens with 0.7 (d) and 1.0 wt.% (e) Y_2O_3. Although circular dendritic formations were also expected from the specimens with 1.5 (f) and 2.0 wt.% (g) Y_2O_3, coarse grains with different orientations were observed. The surface microstructure showed the formation of dispersoids in a micrometer-sized matrix. The dispersoids had diameter range of about 40–80 μm that were present along the grain boundaries. This process showed the existence of discontinuity in matrix material, generating internal stress.

Table 3 Initial parameters for the structural refinements of the ODS FeNiCrY_2O_3 cast alloy

Crystallographic data	Phase-1	Phase-2
Formula	FeNiCr	Y_2O_3
Space group	Fm-3m (I-225)	Ia-3 (I-206)
Lattice parameter:		
a (Å)	3.599724	10.599373
b (Å)	3.599724	10.599373
c (Å)	3.599724	10.599373
α, β, γ (°)	90, 90, 90	90, 90, 90
Cell volume (Å^3)	46.645262	1,190.804663
Atomic number in unit cell, Z	4	144
Atomic position, x, y, z	Fe1: 0.00, 0.50, 0.50	Y1: 0.26, 0.06, 0.21 Y2: 0.25, 0.00, 0.53 O1: 0.16, 0.33, 0.13
U_o parameter	0.0011	0.19701
Young modulus (GPa) (Moreau, et al., 2008)	198	63.5

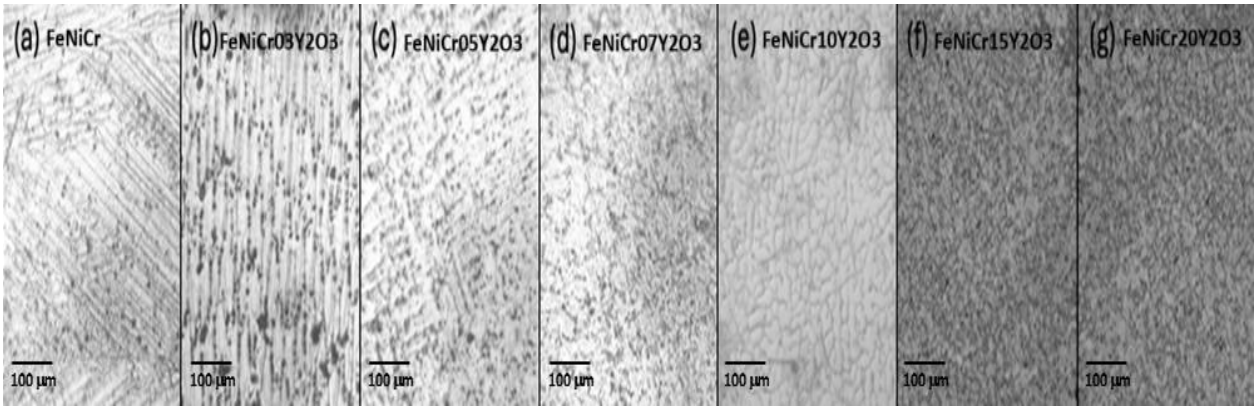

Figure 2 Effect of Y_2O_3 dispersion on microstructure of melt-casted ODS FeNiCrY_2O_3 cast alloys. Optical microscope image with 100x magnification of the inner part of alloys with different dispersion of Y_2O_3: (a) 0.0 wt.%, (b) 0.3 wt.%, (c) 0.5 wt.%, (d) 0.7 wt.%, (e) 1.0 wt.%, (f) 1.5 wt.%, and (g) 2.0 wt.%

Figure 3 showed grain fineness achieved through cast fusion process under austenitic FeNiCr melting conditions (approximately 1450 °C). This method effectively and compactly bonded Y_2O_3 oxide in cast ODS alloy, which contrasted sharply with ODS produced by conventional powder metallurgy methods. The metallurgy method included cold sintering (CS), metal sintering (MS), extrusion (XTR), hot pressing (HP), hot isostatic pressing (HIP), and spark plasma sintering (SPS). (Kishorekumar et al., 2018). In addition, the image showed that alloys without Y_2O_3 had needle-like grains, signifying a high degree of directional compaction. As dispersion of Y_2O_3 increased, the needle-like grains were transformed into cycle-like dendritic formations with wider grain boundaries, which showed more isotropic compaction and higher resistance to grain growth.

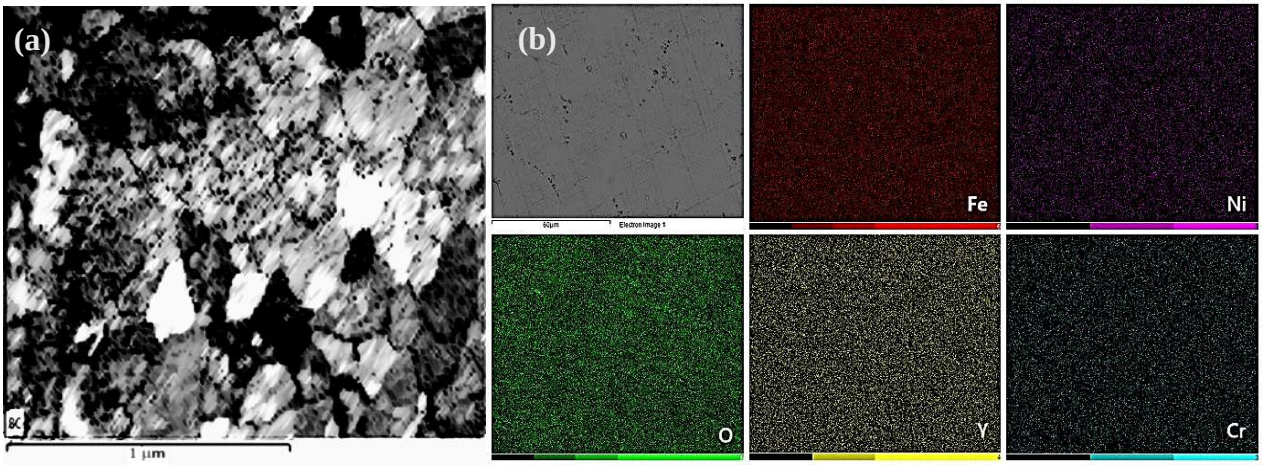

Figure 3 (a) SEM image showing the structure of -FeNiCr matrix and yttria clusters, featuring an average globular austenite grain size of approximately ~1.1 microns, with dispersion of nano oxides both in the grains and along grain boundaries. (b) EDS mapping observation of the inner part of melt-casted ODS FeNiCr10Y_2O_3 alloys

The image showed the uniform dispersion of Y elements, which were strongly associated with Fe. This signified the effectiveness of pre-linking method for achieving homogeneous distribution of Y_2O_3 in alloys. Elemental analysis enumerated that, Fe, Ni as well as Cr had about 23.21, 57.09, and 16.55 wt.%, respectively. In addition, Y (yttrium) about 1.32 wt.%, and O (oxygen) having approximately 1.83 wt.% contributed to system of alloys, signifying the content of Y_2O_3.

3.1.2. SEM/EDS observation

Based on SEM observation of specimens of FeNiCr alloys with different ODS compositions (0 – 2.0 wt.% Y_2O_3), the analysis found that the specimens showed similar morphology as implied by LOM observation. In addition to the process, EDS mapping of these specimens signified interesting results related to the correlation of Fe and Y dispersion. Figure 3 showed SEM/EDS mapping of melt-casted FeNiCrY_2O_3 ODS alloys with 1.0 wt.% Y_2O_3 dispersion. Similar EDS mapping results were observed from all specimens with Y_2O_3 content. Moreover, element mapping of Y looks closely related to Fe, which signified the effectiveness of pre-linking method for achieving a homogeneous distribution of Y_2O_3 in alloys.

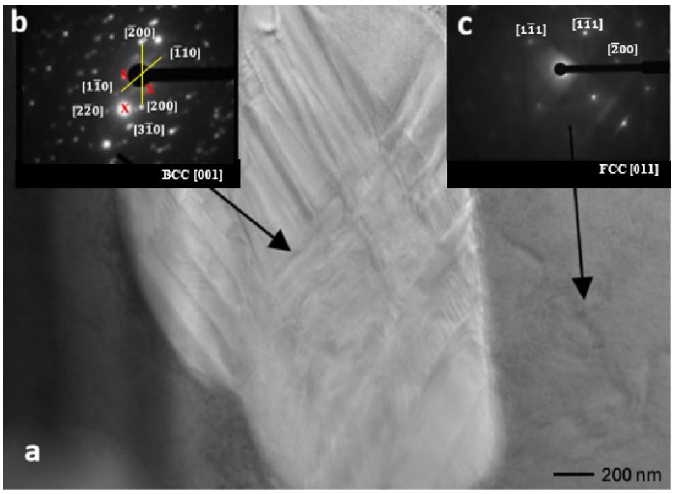

Figure 4 (a) TEM image of FeNiCr10Y_2O_3 alloys showing structural identification of matrix and dispersoid in a few nanometers, (b) and (c) showed indexed diffraction pattern for a BCC [001] and FCC [011] crystals (Globalsino, n.d.). The spacing ratio of the main points was shown as well as the angle between normal planes of the main planes, 45◦ for zone [001] and 54.74◦ [011], respectively. Moreover, the forbidden reflections (b) in zone [001] were shown by the red-cross outside 45◦ angle path. The outcome was due to cubic Y_2O_3 bixbyite structure with C2 and C3i/S6 symmetry sites (Jadhav et al., 2017; Gaboriaud et al., 2015)

3.1.3. TEM observation

FeNiCrY_2O_3 cast alloys were developed by melt casting methods in an argon atmosphere. Minimal amounts of yttria nano-dispersion were incorporated into alloys, forming a 'matrix-cluster' crystal composite cast alloy. In addition, the 'matrix-cluster' arrangements were FeNiCr austenite (FCC) and Y_2O_3 oxide (cubic), including crystalline phases that grew in alloy. The morphology and mapping of alloys showed a stable ODS structure with 'globular' yttria dispersed fragmentarily in it. During the process, individual melting temperatures and densities were significantly different. The yttria was not compounded to form fused materials, as it still stood alone as clusters in a complex cubic phase. Figure 4 showed TEM image of inter-alloying between Y_2O_3 and austenitic matrix in FeNiCr10Y_2O_3 ODS cast alloys. A similar microstructure was expected for the other specimen of ODS alloys with different Y_2O_3 contents. TEM image showed a coarsening of cubic Y_2O_3 particles in the center of the austenitic matrix. Moreover, the selected region diffraction patterns of austenitic matrix and cubic Y_2O_3 particles were obtained along [011] as well as [001] crystallographic directions. These two phases formed the composite structure of ODS cast alloy. The discontinuity in crystal structures caused a lattice stretching dynamic in materials.

TEM in Figure 4(a) showed that the size of Y_2O_3 dispersoid was in the micrometer range, as shown by brighter region in the image. Diffraction pattern obtained from Y_2O_3 region signified BCC [001] zone axis pattern based on the database, shown by 45◦ angle formed by diffraction vectors [$\bar{2}$00] and [$\bar{1}$10] in Figure 4(b) (Globalsino, n.d.). Moreover, forbidden reflections were observed,

marked by red cross in Figure4(b), from cubic Y_2O_3 bixbyite structure with C2 and C3i/S6 symmetry sites. (Jadhav et al., 2017; Gaboriaud et al., 2015). Diffraction pattern from matrix region in Figure 4(c) showed FCC [011] structure as identified in the database. This outcome was signified by 54,74° angle formed through diffraction vectors [$\bar{2}$00] and [$\bar{1}\bar{1}$1]. This outcome was expected from FeCrNi matrix which commonly had FCC crystal structure (Fussik et al., 2018; Williams and Carter, 2009). Figure 4(a) showed that alloys had a combined austenite-FeNiCr (fcc) structure along [011] crystallographic direction, while cubic-yttria crystals were oriented near [001], as signified by the black bars blocking direct beam. These two phases had different thermal properties and interacted with each other, causing the rise of internal stress in ODS casting alloy. Panels in 4(b)-(c) showed the indexing of selected Brag reflection patterns obtained from cubic lattice in 4(a). The simple reciprocal chamber of cubic shown in 4(b) had a simple cubic diffraction pattern. Therefore, there were some forbidden reflections in [001] axis zone, arising from complex multi-atomic unit cell structures (Jin and Kim, 2021; Gaboriaud et al., 2015). Following the discussion, the hkl-reflections in during this analysis took any integer. In Figure 4(c), the pattern at zone axis [011] matched FCC pattern. During the research, indexing spots explained how to identify the selected Brag reflection patterns to determine Miller indices crystal planes (Williams and Carter, 2009). Cubic lattice shown in 4(c), raised face centered diffraction patterns, allowing Bragg reflection to have h+k+l=2n. The difference between indexing of Bragg peaks in 4(b) and 4(c) was due to lattice types, which were I as well as P for panels in 4(b) and 4(c) respectively (Olaoye, 2015).

3.2. Rietveld Analysis

3.2.1. $FeNiCrY_2O_3$ ODS cast alloys profiles

Figure 5 (a) showed neutron diffraction patterns of $FeNiCrY_2O_3$ ODS cast alloys with the 2θ ranging from 40° to 130°. FeNiCr alloys signified a face-centered cubic (fcc) crystal system reviewed by five main diffraction peaks. Additionally, the corresponding planes were (111), (200), (220), (311), and (222), which appeared at the 2θ angles of 51°, 60°, 91°, 114°, as well as 122°, respectively. The austenite diffraction showed distinctive pattern and had different scattering plane from ferrite diffraction pattern, which was body-centered cubic crystal system (Parikin et al., 2018). Moreover, the addition of Y_2O_3 slightly changed diffraction patterns observable in peak shifting, intensity changing, and peak broadening. These effects were attributed to the variation of Y_2O_3 dispersion in alloys. Figure 5 (b) showed that these effects also occurred in the primary peak (111), signifying changes in the lattice structure and strains of alloys.

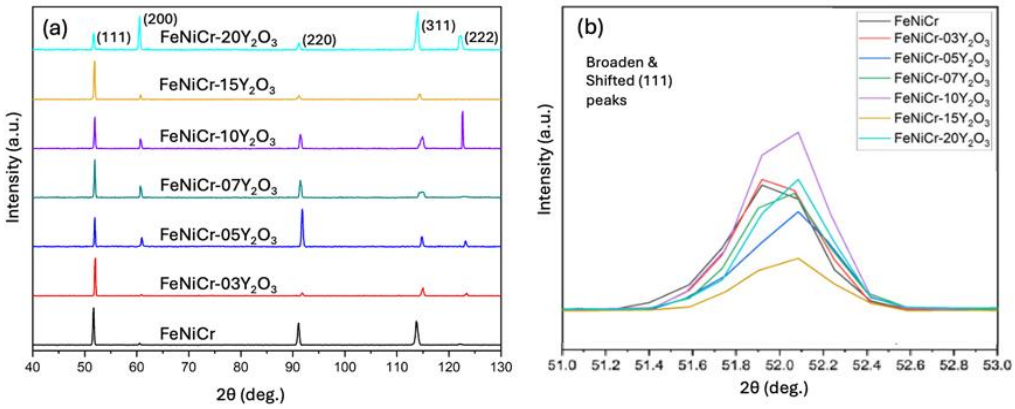

Figure 5 HRPD patterns of FeNiCr cast alloys with varying concentrations of Y_2O_3, showing peak intensities and positions. (a) HRPD patterns of FeNiCr cast alloys with Y_2O_3 content ranging from 0 to 2.0 wt.% from 2θ at 40 to 130 degrees. Moreover, the peaks were sharp and distinct, with variations in intensity as well as position depending on the concentration of Y_2O_3. (b) A zoomed-in version of HRPD patterns focused on a specific range of 2θ angles from around 51.0 to 53.0 degrees.

These data showed the effect of Y_2O_3 on changing lattice parameters of FeNiCr cast alloys, which were also strongly related to residual stress.

3.2.2. Refined parameters

Table 4 showed the refined parameters, namely, lattice, mass, and volume fractions of the phases. The mass fraction of cubic Y_2O_3 in the specimens increased with its addition to the composition, while the volume fraction of Y_2O_3 appeared to be randomly computed due to the separation of materials. All neutron diffraction profiles of the specimens were successfully refined with a goodness of fit (GOF) reliability ranging from 1.16 to 1.48.

Table 4 Refined ambient-temperature lattice parameters and phase fractions of ODS FeNiCrY_2O_3 specimens

Specimen Code	Y_2O_3 (wt.%)	*GOF* (%)	Lattice Parameters (Å)		Mass Fraction (w%)		Volume Fraction (f%)	
			FeNiCr (Austenite Matrice)	Y_2O_3 (Cubic-Yttria)	FeNiCr (Austenite Matrice)	Y_2O_3 (Cubic-Yttria)	FeNiCr (Austenite Matrice)	Y_2O_3 (Cubic-Yttria)
FeNiCr	-	1.20	3.59783	-	100.00	-	1.00000	-
FeNiCr-03Y_2O_3	0.3	1.16	3.59069	10.61221	99.65	0.35	0.99865	0.00135
FeNiCr-05Y_2O_3	0.5	1.19	3.59529	11.39172	99.41	0.59	0.99522	0.00478
FeNiCr-07Y_2O_3	0.7	1.22	3.59929	10.55049	99.30	0.70	0.99367	0.00633
FeNiCr-10Y_2O_3	1.0	1.41	3.59746	10.59284	98.82	1.18	0.99968	0.00324
FeNiCr-15Y_2O_3	1.5	1.46	3.60936	10.65735	98.48	1.52	0.98937	0.01063
FeNiCr-20Y_2O_3	2.0	1.48	3.67214	10.79821	97.93	2.06	0.96686	0.03314
Y_2O_3	100.0	1.40	-	11.48965	-	100.00	-	1.00000

3.2.3. Strain tensor properties

The refinements produced GOF with σ between 1.16 and 1.48 to diffraction data for each specimen. The experimental precision identified that the volume-averaged lattice strains along various [hkl] agreed with the crystal symmetry. This process was expected for the strains arising solely from the mismatch of thermal expansion in a mixture of randomly oriented grains. Since the strain tensor conformed to crystal symmetry, the number of independent components reduced to one. When analysis uniaxial crystal structures, such as in austenite matrices and Y_2O_3 structures, an independent component sufficed to represent the strain tensor properties completely (Newnham, 2020). Along any other direction, the strains were computed using the tensor algebra (De Prunelé et al., 2007). The process was desirable to determine strain components along principal axes, which were the a-axis for austenite matrix phase and cubic Y_2O_3 phase in conventional structure setting.

3.2.4. Thermal expansion mismatch

Table 5 showed that austenite matrix and FeNiCrY_2O_3 ODS cast alloys were initially in a compression and then gradually in a tension after exceeding a composition of 1.0 wt.% Y_2O_3. Meanwhile, Y_2O_3 phase signified compressive tendency for entire composition.

The strains measured in each phase were highly isotropic and stretching in materials was dominated by strain behavior of matrix (FeNiCr) phase. These features were qualitatively explained by considering thermal expansion mismatch between austenite matrix and Y_2O_3 particles exchanging expansion when heating was applied during smelting (Kim et al., 2019; Koh et al., 2013).

Table 5 Average lattice strains and hydrostatic stress along major crystallographic directions (*a*-axis) of the ODS FeNiCrY_2O_3 specimens

Specimen Code	Average Lattice Strain, □ (%)			Hydrostatic Stress, □ (GPa)
	a// FeNiCr (Austenite Matrice)	*a*// Y_2O_3 (Cubic Yttria)	ODS FeNiCrY_2O_3 (*a*// resultant)	
FeNiCr	0	0	0	0
FeNiCr-03Y_2O_3	-0.198185045	-0.010309661	-0.208494706	-98.80982917
FeNiCr-05Y_2O_3	-0.070260652	-0.004074148	-0.0743348	-35.19377829
FeNiCr-07Y_2O_3	0.040323145	-0.0517412	-0.011418055	-0.918724427
FeNiCr-10Y_2O_3	-0.010280686	-0.025289407	-0.035570093	-14.79176123
FeNiCr-15Y_2O_3	0.317064344	-0.077002772	0.240061572	121.5717199
FeNiCr-20Y_2O_3	1.996963909	-0.199434461	1.797529447	877.1952868

3.2.5. Lattice strain and residual stress analysis

Figure 6 showed the effect of Y_2O_3 content on lattice strain and residual stress of FeNiCrY_2O_3 ODS cast alloys. As shown in Figure 6 (a), lattice strain of FeNiCrY_2O_3 ODS phase increased with higher Y_2O_3 content, while latter remained unchanged. The outcome signified that Y_2O_3 dispersion induced significant distortion in the lattice of FeNiCrY_2O_3 ODS phase. The result of the process improved strength and hardness of alloys. Similarly, Figure 6(b) showed that residual stress of FeNiCrY_2O_3 ODS phase also increased with higher Y_2O_3 content, having no significant variation in Y_2O_3 phases. This outcome signified that Y_2O_3 dispersion generated a compressive residual stress in FeNiCrY_2O_3 ODS phase, improving the resistance to any crack propagation and some fracture in alloys. Figures 6(a) and (b) showed that lattice strains and residual stress of ODS specimens varied inconsistently when Y_2O_3 contents were less than 1.0 wt.%.

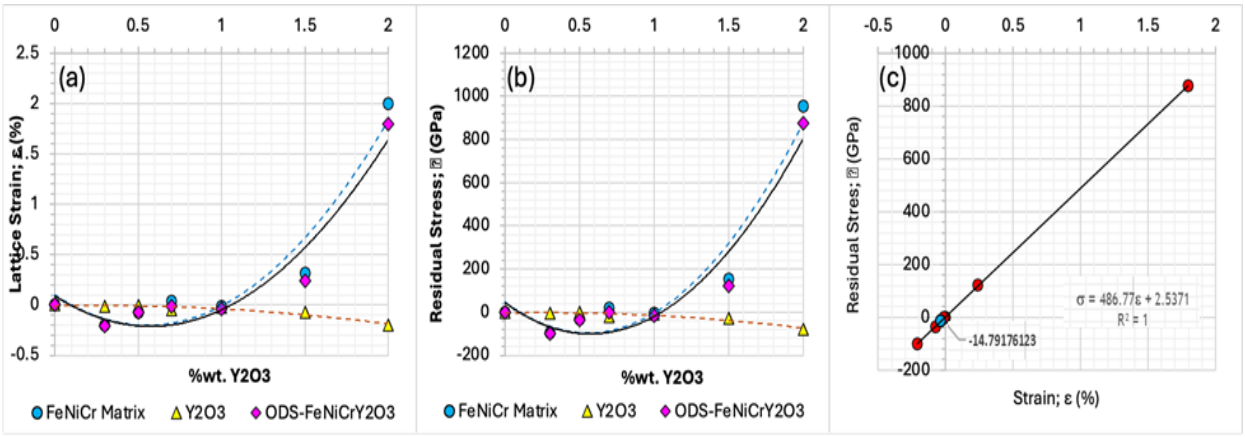

Figure 6 Lattice strain and residual stress analysis of ODS FeNiCrY_2O_3 cast alloys as a function of Y_2O_3 content. The lattice strain and residual stress were calculated from the peak broadening of the patterns using Williamson-Hall method. (a) Average lattice strains along the major crystallographic directions (*a*-axis). (b) Residual stress along the major crystallographic directions (*a*-axis). (c) Equilibrium residual stress-strain curve of alloys.

Strain and stress remained unchanged when Y_2O_3 contents were 1.0 wt.%. However, both increased when the addition of Y_2O_3 was more than 1.0 wt.%. The stretching of parallel crystal lattices a// and b// were distorted to eliminate each other in addition to the morphology and elemental mapping in alloys being better dispersed. Both lattices approached zero when Y_2O_3 content was 1.0 wt.% with a compressive residual stress of about 14.79 GPa. The compressive stress under compositional equilibrium predicted that 1.0 wt.% Y_2O_3 was considered stable in FeNiCrY_2O_3 ODS cast alloy, and it showed excellence for further production.

Figure 6 (c) showed the relationship between residual stress and lattice strain for each phase. A linear relationship was observed, signifying that residual stress and lattice strain were proportional to each other. In addition, the slope of line represented elastic modulus of the phase, which reflected the stiffness of materials (Parikin and Allen, 2015; Yang et al., 2023). FeNiCr10Y_2O_3 ODS phase had its strain and residual stress almost zero. This outcome showed that optimum Y_2O_3 content in 58Fe25Ni17Cr alloys was about 1.0 wt.%. Among the four alloys containing Y_2O_3 oxide signifying compressive residual stress behavior, the most moderate type recommended for further fabrication as FeNiCrY_2O_3 ODS system was 57Fe25Ni17Cr1.0Y_2O_3 cast alloy.

4. Conclusions

In conclusion, this research investigated the effect of Y_2O_3 dispersion on the micro-crystal structure and residual stress of FeNiCrY_2O_3 ODS cast alloys. Alloys were synthesized by mechanical alloying and arc melt-casting methods as well as characterized by neutron diffraction and various microscopy methods. The results showed that Y_2O_3 dispersion induced a lattice compression in austenitic FeNiCr matrix, which implied a tensile residual stress in the crystals. Moreover, the distribution of residual stress in alloys was related to individual mechanical properties and performance. Optimum Y_2O_3 content in this type of FeNiCrY_2O_3 ODS cast alloys was estimated to be about 1.0 wt.%, which showed better nano-dispersion and signified lowest strain and residual stress. The compressive stress of 14.79 GPa at strain equilibrium (ε~0) was considered to be stable in this ODS cast alloys and excellent for further production in 57Fe25Ni17Cr1.0Y_2O_3 system.

Acknowledgments

The authors are grateful to our mentors, Prof. Dr. Syahbuddin from University of Pancasila, Dr. Abu Khalid Rivai, Dr. Iwan Sumirat, and Dr. Dany Mulyana, from Badan Riset dan Inovasi Nasional (BRIN), for individual advice and guidance throughout this research. The authors are also grateful to BRIN-Advanced Physic Laboratory Facility and Prof. Dr. Agus Eddy Basuki from Faculty of Metallurgical, Mining, and Petroleum Engineering at Bandung Institute of Technology (ITB) for individual helpful recommendations, as well as kindness. Part of this research was conducted in Research Center for Nanoscience and Nanotechnology, ITB, and the authors are grateful to the center for providing the necessary facilities as well as resources. The authors acknowledge the financial support from Degree by Research Program of BRIN, in partnership with Department of Metallurgy and Materials Engineering, Faculty of Engineering, University of Indonesia, Depok. This research is fully funded by Research and Innovation for Advanced Indonesia (RIIM-G.3) program for fiscal year 2023 from LPDP.

Author Contributions

Parikin Farihin: conceptualization, data curation, formal analysis, investigation, methodology, project administration, validation, writing-original draft, and writing-review & editing.
Bambang Suharno: supervision and project administration.
Ferhat Aziz: writing-review & editing and funding acquisition.
Mohammad Dani: supervision, project administration and resources.
I Wayan Ngarayana: visualisation, writing-review & editing and funding acquisition.
Andryansyah: supervision, validation, data curation and methodology.
Andon Insani: data curation and funding acquisition.
Rai Indra Wardana: data curation and funding acquisition.
Damar Rastri Adhika: formal analysis, methodology and investigation.
Ching An Huang: supervision.

Conflict of Interest

There are no conflicts of interest to disclose.

References

Andoko, A., Kurniawan, P., Suprayitno, S., Gapsari, F., Manawan, M 2024. Residual Stress and Texture Analysis of Leaf Spring Failure. *International Journal of Technology,* vol. 15, no. 4, pp. 1162-1172, https://doi.org/10.14716/ijtech.v15i4.5571

Arshad, M, Amer, M, Hayat, Q, Janik, V, Zhang, X, Moradi, M & Bai, M 2022, 'High-Entropy Coatings (HEC) for high-temperature applications: materials, processing, and properties', *Coatings*, vol. 12, no. 5, pp. 691-725, https://doi.org/10.3390/coatings12050691

Aziz, F, Rivai, AK, Mardiyanto, P, Dani, M & Suharno, B 2024, 'Accident tolerant fuel cladding materials for light water reactors: analysis of neutronic characteristics', *International Journal of Technology*, vol. 15, p. 608, https://dx.doi.org/10.14716/ijtech.v15i3.5345

Brewer, LN, Bennett, MS, Baker, BW, Payzant, EA & Sochalski-Kolbus, LM 2015, 'Characterization of residual stress as a function of friction stir welding parameters in oxide dispersion strengthened (ODS) steel MA956', *Materials Science and Engineering*, vol. A-647, pp. 313–321, https://doi.org/10.1016/j.msea.2015.09.020

Buckthorpe, D 2017, 'Introduction to Generation IV nuclear reactors', In: *Structural Materials for Generation IV Nuclear Reactors*, ed. P Yvon, Woodhead Publishing, pp. 1-22, https://doi.org/10.1016/B978-0-08-100906-2.00001-X

Dani, M, Dimyati, A, Parikin, Adhika, DR, Jahja, AK, Insani, A, Syahbuddin, Huang, CA 2019, 'Microstructure and Deformation of 57Fe17Cr25NiSi Austenitic Super Alloy After Arc Plasma Sintering', *International Journal of Technology*, vol. 10, no. 5, pp. 988-998, https://dx.doi.org/10.14716/ijtech.v10i5.2991

Dani, M, Mustofa, S, Parikin, Sumaryo, Sudiro, T, Hermanto, B, Adhika, DR, Insani, A, Dimyati, A, Syahbuddin, Hardjanto, S, Basuki, EA & Huang, CA 2020, 'Effect of Spark Plasma Sintering (SPS) at temperatures of 900 and 950 oc for 5 minutes on microstructural formation of fe-25ni-17cr austenitic stainless steel', *IJETER*, vol. 8, pp. 4845–4853, https://doi.org/10.30534/ijeter/2020/124882020

De Prunelé, E 2007, 'Linear strain tensor and differential geometry', *American Journal of Physics*, vol. 75, pp. 881–887, https://doi.org/10.1119/1.2750376

Dong, Q, Xu, G, Hu, Y & Peng, Z 2023, 'Research on the residual strength of cracked plate considering fatigue crack propagation under cyclic load', *JMSE*, vol. 11, no. 4, pp. 706-821, https://doi.org/10.3390/jmse11040706

Du, B., Wen, J., Ru, Y., Hu, Y., Yang, F., Cao, Y. Geng, L., Pei, Y., Li, S. & Gong, S 2024. Role of dislocation behavior during aging in high-temperature microstructural evolution and creep property of single crystal superalloys, 'Materials Science and Engineering: A', vol. 916, article 147384, https://doi.org/10.1016/j.msea.2024.147384

Em, V., Ivan, K., Woo, W. & Mikula, P 2024, Neutron diffraction measurements of residual stresses for ferritic steel specimens over 80 mm thick, 'Metals', vol. 14, no. 6, article 638, https://doi.org/10.3390/met14060638

Fussik, R, Walter, M, Theisen, W & Weber, S 2018, 'Investigation of austenitic FeCrNi steels with regard to stacking-fault energy and thermal austenite stability', *Materialia*, vol. 3, pp. 265-273, https://doi.org/10.1016/j.mtla.2018.08.020

Gaboriaud, RJ, Paumier, F & Lacroix, B 2015, 'Disorder–order phase transformation in a fluorite-related oxide thin film: In-situ X-ray diffraction and modelling of the residual stress effects', *Thin Solid Films*, vol. 601, https://doi.org/10.1016/j.tsf.2015.08.030

Globalsino n.d., Standard indexed diffraction patterns for bcc crystals: - practical electron microscopy and database -an online book-, Viewed 01 January 2025, (https://www.globalsino.com/EM/page3916.html)

Gougar, HD, Petti, DA, Demkowicz, PA, Windes, WE, Strydom, G, Kinsey, JC, Ortensi, J, Plummer, M, Skerjanc, W, Williamson, RL, Wright, RN, Li, D, Caponiti, A, Feltus, MA & O'Connor, TJ 2020, 'The US Department of Energy's high temperature reactor research and development program – Progress as of 2019', *Nuclear Engineering and Design*, vol. 358, pp. 1-15, https://doi.org/10.1016/j.nucengdes.2019.110397

Guo, Y, Li, M, Li, P, Chen, C, Zhan, Q, Chang, Y & Zhang, Y 2020, 'Microstructure and mechanical properties of oxide dispersion strengthened FeCoNi concentrated solid solution alloys', *Journal of Alloys and Compounds*, vol. 820, pp. 1-16, https://doi.org/10.1016/j.jallcom.2019.153104

Jadhav, A, Khan, S, Kim, S, Lee, SY, Park, JK & Cho, SH 2017, 'Near-infrared quantum cutting in Tb3+ and Yb3+-doped Y2O3 nanophosphors', *Research on Chemical Intermediates*, vol. 43, https://doi.org/10.1007/s11164-016-2427-9

Jin, J & Kim, J 2021, 'Structure and Photoluminescence of optically transparent Y_2O_3: Eu thin films prepared on sapphire substrates by RF magnetron sputtering', *Applied Science and Convergence Technology,* vol. 30, pp. 34-37, https://doi.org/10.5757/ASCT.2021.30.1.34

Kim, SY, Lim, JH, Shin, HS, Yeo, DH & Yoon, HG 2019, 'Effects of Y_2O3 additive on mechanical and thermal properties of cordierite-mullite ceramics', *Journal of Nanoscience and Nanotechnology,* vol. 19, pp. 1580–1584, https://doi.org/10.1166/jnn.2019.16248

Kishorekumar, P., Vijaya Sai, N, Gopala Krishna, A & Renganathan, NG 2018, 'Consolidation of nano-oxide dispersion strengthened austenitic stainless steels for high temperature applications: a review', *Manufacturing Technology Today*, vol. 17, no. 12, pp. 12–20, http://mtt.cmti.res.in/index.php/journal/article/view/304

Koh, JH, Sorge, E, Wen, TC & Shetty, DK 2013, 'Thermal expansion behaviors of yttrium tungstates in the WO_3–Y_2O_3 system', *Ceramics International*, vol. 39, pp. 8421–8427, https://doi.org/10.1016/j.ceramint.2013.04.024

Kühne, D, Spak, B, Kästner, M, Brosius, A & Fiedler, M 2021, 'Consideration of cyclic hardening and residual stresses in fatigue life calculations with the local strain approach', *Archive of Applied Mechanics*, vol. 9, pp. 3693–3707, https://doi.org/10.1007/s00419-021-01950-0

Li, W, Xu, H, Sha, X, Meng, J & Wang, Z 2019, 'Microstructure and mechanical properties of 14Cr-ODS steels with Zr addition', *High Temperature Materials and Processes*, vol. 38, pp. 404–410, https://doi.org/10.1515/htmp-2018-0067

Lutterotti, L 2000, 'Maud: A Rietveld analysis program designed for the internet and experiment integration', *Acta Crystallogr. A Found Crystallogr*, vol. A56, S54, https://doi.org/10.1107/S0108767300021954

Mo, F, Sun, G, Li, J, Zhang, C, Wang, H, Chen, Y, Liu, Z, Yang, Z, Li, H, Yang, Z, Pang, B, Huang, Y, Tian, Y, Gong, J, Chen, B & Peng, S 2018, 'Recent progress of residual stress distribution and structural evolution in materials and components by neutron diffraction measurement at RSND', *Quantum Beam Science*, vol. 2, no. 3, pp. 15-33, https://doi.org/10.3390/qubs2030015

Moreau, A, Kruger, S, Côté, M & Bocher, P 2008, 'In-situ monitoring of microstructure during thermomechanical simulations using laser-ultrasonics', *e-Journal of Nondestructive Testing*, vol. 13, no. 10, https://www.ndt.net/?id=6931

Mustofa, S, Dani, M, Parikin, Sudiro, T, Hermanto, B, Adhika, DR & Syahbuddin, Huang, CA 2020, 'Effect of temperature of spark plasma sintering on the development of oxide compound in Fe-25wt%Ni-17wt%Cr Austenitic Stainless Steel', *International Journal of Emerging Trends in Engineering Research*, vol. 8, pp. 5661–5667, https://doi.org/10.30534/ijeter/2020/122892020

Naserinejad, K, Masoumi, A, Bor, TC & Mashhadi, MM 2024, 'Numerical and Experimental Investigation of Residual Stress and Bond Strength in Friction Surface Cladding Process', *J. of Materi Eng and Perform*, vol. 33, pp. 3859–3870, https://doi.org/10.1007/s11665-023-09041-7

Newnham, RE 2020, 'Stress and strain', in *Properties of Materials: Anisotropy, Symmetry, Structure*, Oxford Academic, Oxford, https://doi.org/10.1093/oso/9780198520757.003.0012

Oka, K, Ohnuki, S, Yamashita, S, Akasaka, N, Ohtsuka, S & Tanigawa, H 2007, 'Structure of Nano-Size Oxides in ODS Steels and Its Stability under Electron Irradiation', *Materials Transactions - MATER TRANS*, vol. 48, pp. 2563-2566, https://doi.org/10.2320/matertrans.MD200715

Olaoye, O 2015, 'Structural Dynamics in DCNQI Salts and Transition Metal Dichalcogenides Studied by Electron Diffraction Simulation', https://doi.org/10.13140/RG.2.1.1994.2165

Parikin, Dani, M & Sulistioso, GS 2019, 'Review on a new austenitic 57Fe15Cr25Ni stainless steel at temperature of 850C for 30 minutes followed by water quenching treatments', *Malaysian Journal of Fundamental and Applied Sciences*, vol. 15, pp. 651–657, https://doi.org/10.11113/mjfas.v15n5.1299

Parikin, Dani, M, Dimyati, A, Purnamasari, ND, Sugeng, B, Panitra, M, Insani, A, Priyanto, TH, Mustofa, S, Syahbuddin & Huang, CA 2021, 'Effect of arc plasma sintering on the structural and microstructural properties of Fe-Cr-Ni austenitic stainless steels', *Makara Journal of Technology,* vol. 25, no. 2, pp. 71-78, https://doi.org/10.7454/mst.v25i2.3922

Parikin, F, Suharno, B, Dani, M, Andryansyah, A, Prastowo, DA, Insani, A & Prayitno, DH 2024, 'A Novel Processing Route in the Mechano-Synthesis of Austenitic 58Fe25Ni17Cr Oxide Dispersion Strengthened Cast Alloy through Y2O3 Pre-Linking', *Key Engineering Materials Trans Tech Publications, Ltd.*, vol. 975, pp. 29–40, https://doi.org/10.4028/p-1UIqtf

Parikin, Killen, P & Rafterry, A 2009, 'Measurements of residual stresses in cold-rolled 304 stainless steel plates using x-ray diffraction with rietveld refinement method', *Atom Indonesia*, vol. 35, no. 1, pp. 19-36, https://doi.org/10.17146/aij.2009.45

Parikin, P & Allen, D 2015, 'Independency of elasticity on residual stress of room temperature rolled stainless steel 304 plates for structure materials', *Makara Journal of Technology*, vol. 19, no. 3, pp. 97-102, https://doi.org/10.7454/mst.v19i3.3040

Parikin, P, Dani, M, Jahja, A, Iskandar, R & Mayer, J 2018, 'Crystal structure investigation of ferritic 73Fe24Cr2Si0.8Mn0.1Ni steel for multi-purpose structural material applications', *International Journal of Technology*, vol. 9, no. 1, pp. 78-88, https://dx.doi.org/10.14716/ijtech.v9i1.247

Raman, L, Karthick, G & Murty, BS 2016, 'Austenitic oxide dispersion strengthened steels: a review', *Defence Science Journal*, vol. 66, pp. 316-322, https://doi.org/10.14429/dsj.66.10205

Ruan, JL, Pei, Y & Fang, D 2012, 'Residual stress analysis in the oxide scale/metal substrate system due to oxidation growth strain and creep deformation', *Acta Mech*, vol. 223, pp. 2597–2607, https://doi.org/10.1007/s00707-012-0739-4

Statti, G, Mehmanparast, A, Biswal, R & Rizzo, CM 2021, 'Evaluation of cyclic loading effects on residual stress relaxation in offshore wind welded structures', *Journal of Multiscale Modelling*, vol. 12, no. 2, pp. 215-220, https://doi.org/10.1142/S1756973721500050

Tanaka, K, Akiniwa, Y & Hayashi, M 2002, 'Neutron diffraction measurements of residual stresses in engineering materials and components', *Materials Science Research International*, vol. 8, pp. 165-174, https://doi.org/10.2472/jsms.51.12Appendix_165

Was, GS, Petti, D & Ukai, S 2019, 'Materials for future nuclear energy systems', *Journal of Nuclear Materials*, vol. 527, p. 151837, https://doi.org/10.1016/j.jnucmat.2019.151837

Williams, DB & Carter, CB 2009, *Transmission Electron Microscopy: A Textbook for Materials Science*, Springer, https://link.springer.com/book/10.1007/978-0-387-76501-3

Xu, R., Li, Y. & Yu, H 2023. Microstructure Evolution and Dislocation Mechanism of a Third-Generation Single-Crystal Ni-Based Superalloy during Creep at 1170 °C. Materials. 16. 5166. 10.3390/ma16145166.

Yan, J-J., Li, J., Yang, Z-L., Gu,R-N., Yan, M. & Quach, W-M 2022. Neutron diffraction residual stress analysis and mechanical properties of additively manufactured high strength steel hollow sections, Thin-Walled Structures, Volume 179, 109729. https://doi.org/10.1016/j.tws.2022.109729

Yang, WK, Song, ZM, Luo, XM & Zhang, GP 2023, 'Evaluation of tensile and fatigue properties of metals using small specimens', *Acta Metallurgica Sinica (English Letters)* ,vol. 36, pp. 147–157, https://doi.org/10.1007/s40195-022-01456-w

Yusupandi, F., Ilham, M., Yafi, I.A., Widiatmoko, P., Nurdin, I., Febrianti Khairunnisa, S., Devianto, H 2024, Improvement of anode supported intermediate temperature solid oxide fuel cell with spray-coated calcia-stabilized zirconia electrolytes*, International Journal of Technology,* vol. 15, no. 6, pp. 1971-1981, https://doi.org/10.14716/ijtech.v15i6.6308

Zang, P, Zhang, G, Chen, Z, Chen, H, Huang, Y, Yi, M, Tian, C, Zhang, R, Wang, L & Xu, C 2024, 'Finite element analysis of residual stress toughening Al2O3/TiC/TiB2/h-BN@Al2O3 composite ceramic materials', *Journal of Materials Research*, vol. 39, pp. 789–800, https://doi.org/10.1557/s43578-023-01269-2

Zhang, H., Shao, B., Chen, H., Wang, P., Song, X., Vairis, A. & Li, W 2024, 'A novel method to relieve residual stress in dissimilar brazed joints via micro-scale additive manufacturing', *Ceramics International,* vol. 50, no. 22, Part C, pp. 48832-48842, https://doi.org/10.1016/j.ceramint.2024.09.238

Zhang, S, Yingchun, S, Barsotti, D & Gray, G 2019, 'Thermal considerations for information technology equipment from product safety perspective', *Conference: 2019 IEEE Symposium on Product Compliance Engineering (SPCE Austin)*, pp. 1-9, https://doi.org/10.1109/SPCE47297.2019.8950824

Zinkle, SJ & Was, G 2013, 'Materials Challenges in Nuclear Energy', *Acta Materialia*, vol. 61, pp. 735–758, https://doi.org/10.1016/j.actamat.2012.11.004